

Non-linear free periodic vibrations of open cylindrical shallow shells

P. Ribeiro*

IDMEC/DEMEGI, Faculdade de Engenharia, Universidade do Porto, rua Dr. Roberto Frias, s/n, 4200-465 Porto, Portugal

Received 10 January 2007; received in revised form 19 October 2007; accepted 14 November 2007

Available online 10 January 2008

Abstract

This paper is concerned with the non-linear free periodic vibrations of thin, open, cylindrical and shallow shells vibrating in the geometrically non-linear regime. A multi-degree-of-freedom model with hierarchical basis functions is adopted and the principle of the virtual work is used to define the time domain equations of motion. These equations are transformed into the frequency domain by the harmonic balance method and are finally solved by an arc-length continuation method. Shells of different thicknesses and of different curvature radius are analysed, and the variation of the non-linear natural frequencies of these shells with the vibration amplitude are investigated in some detail. The variation of the mode shapes with the vibration amplitude is demonstrated. It is found that both softening and hardening spring effects occur and that the number of couplings between vibration modes is rather large in undamped shells.

© 2007 Elsevier Ltd. All rights reserved.

1. Introduction

The problem here considered is the free periodic oscillation of open cylindrical shells with large displacements. Unlike in linear systems, the natural modes of vibration of geometrically non-linear shells are constituted by amplitude-dependent mode shapes and amplitude-dependent natural frequencies of vibration. Therefore, the analysis of free periodic oscillations is quite more complex than in the linear case and all published studies resort to approximations of some sort.

If the shells are shallow, that is with large length-to-radius ratio, it is possible to use equations in Cartesian coordinates which are very similar to the ones of flat panels, but with additional terms in order to account for the initial curvature. Due to their relative simplicity, the application of shallow shell theories to investigate free periodic vibrations are rather popular. Leissa and Kadi [1] followed a shallow shell theory in order to study the effect of the curvature upon the natural vibration frequencies of thin shells of rectangular planform and supported by shear diaphragms. The analysis was extended to the non-linear regime by means of the Galerkin procedure and numerical integration in time; most of the shells studied presented initially a softening spring effect, which was followed by hardening spring. It was assumed that the non-linear mode shape does not vary

*Tel.: +1 351 22 508 1716; fax: +1 351 22 508 1445.

E-mail address: pmleal@fe.up.pt

with amplitude and the model had one generalised coordinate for each displacement component. In Ref. [2] the free vibrations of simply supported shallow shells of rectangular planform were investigated. It was assumed that the transverse oscillations have a sinusoidal form with half a wave in the x and y directions, and Airy stress function was employed; furthermore, harmonics either than the first and third were neglected in the time series. Softening followed by hardening was found in most of the shells analysed. In Ref. [3] the effect of the thickness and the curvature upon the large-amplitude free vibrations of shallow shells supported by shear diaphragms was studied. A model with one degree of freedom per displacement component was used as in Ref. [1], but first-order shear deformation theory was followed. It was concluded, as in Refs. [1,2], that most shells present soft spring behaviour for small vibration amplitude, followed by hardening spring. More works have been published where a one-degree-of-freedom model was used to study free vibrations of shells (for example, Refs. [4,5]).

Publications also exist where several degrees of freedom were employed to define the spatial models of shells. A first-order shear deformation, p -version finite element with hierarchic basis functions for moderately thick, isotropic shallow shells was presented in Ref. [6] and a preliminary investigation was carried out. The goals of the latter research were to show that the p -version finite element method requires a small number of degrees of freedom and that the mode shapes change with the amplitude of vibration. It was possible to achieve these goals assuming that the oscillations remain harmonic, but this is a severe restriction, particularly for shells of smaller curvature radius. Modal formulations for large-amplitude free vibration of shells were suggested in Ref. [7], where first-order shear deformation theory was also followed. The authors concluded that, even for moderate deflections, the higher modes contribution can be quite large. In Ref. [8] the forced vibrations of simply supported panels were investigated. Direct time integration and an arc-length continuation method were employed and internal resonances were found. In Ref. [9] vibrations of circular cylindrical open shells subjected to harmonic excitation were numerically and experimentally analysed. The effect of geometric imperfections on the trend of non-linearity and on natural frequencies was investigated. Moreover, the phenomenon of one-to-one internal resonance has been detected and investigated numerically on one of the panels studied.

Readers interested in wider reviews on vibration of circular cylindrical shells and shallow shells should consult Refs. [10,11].

The goals of the present paper are to examine the periodic geometrically non-linear vibrations of isotropic, linear elastic, thin, open circular cylindrical shallow shells, to study the frequency and mode shape dependence on the vibration amplitude and to illustrate the internal resonances that occur between non-linear modes. To derive the mathematical model a procedure similar to the one presented in Ref. [6] is followed. However, because only rather thin panels are here considered, a Kirchhoff-type model is adopted instead of the first-order shear deformation model followed in Ref. [6]. Modal coordinates are employed in order to reduce the number of equations. However, several linear modes are included, since severe reduction of the number of coordinates would not only restrain the ability to describe the variation of the non-linear mode shapes with the vibration amplitude, but also fail to correctly predict their interaction. The harmonic balance method is applied to transform the equations of motion into the frequency domain, using a truncated series with a constant term and three harmonics, and the resulting equations are solved by a continuation method.

2. Formulation

The equations of motion are obtained by employing the principle of the virtual work, following a procedure which is common in p -version finite element models [6,12–17]. It is assumed that the shells are thin, elastic, isotropic, shallow and that their projection in a plane is rectangular (Fig. 1). Their undeformed geometry is defined from a reference plate by introducing an initial displacement $w^i(x, y)$, which is small in comparison with the spans. Therefore, the curvilinear coordinates commonly employed in shells can be directly replaced by the Cartesian coordinates x and y , and the Lamé parameters are $A = B = 1$ [18,19]. The strain–displacement relations of shallow shells are only slightly more complicated than the ones of plates.

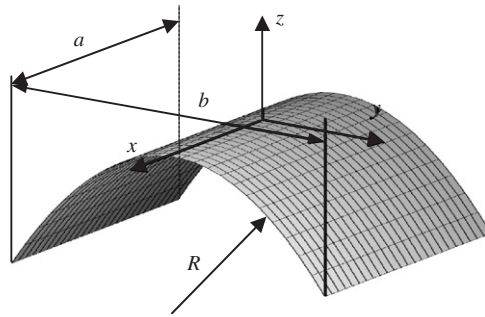


Fig. 1. Cylindrical shallow shell with rectangular planform.

In a three-dimensional, rectangular coordinate system, which is orientated so that R is the principal curvature radius—Fig. 1—the middle surface of the shallow shell is expressed as

$$w^i(x, y) = -\frac{1}{2} \left(\frac{y^2}{R} \right). \quad (1)$$

The dimensions a and b , which are the lengths of the projection of the shell in a plane, are represented in Fig. 1; the constant thickness will be represented by h .

Since only thin shells will be analysed, the transverse shear deformation is neglected and it is assumed that normals to the middle surface suffer no extension. Hence, the displacement components u and v , of a particle along the x and y directions are functions of the middle surface membrane displacements u^0 , v^0 , and of the rotations of the normal to the middle surface about the x - and y -axis, being the latter simply $\theta_y = -w_{,x}^0$ and $\theta_x = w_{,y}^0$. w^0 is the middle surface component of displacement along the z direction, defined in relation to the initial configuration given by Eq. (1). The comma indicates partial differentiation and the superscript “0” represents the middle surface. The displacement components of a particle located at (x, y, z) are therefore given by

$$u(x, y, z, t) = u^0(x, y, t) - zw_{,x}^0(x, y, t), \quad (2)$$

$$v(x, y, z, t) = v^0(x, y, t) - zw_{,y}^0(x, y, t), \quad (3)$$

$$w(x, y, z, t) = w^0(x, y, t). \quad (4)$$

It is here assumed that the middle plane displacement components— u^0 , v^0 and w^0 —depend on the coordinates x, y and on the vector of generalised displacements $\mathbf{q}(t)^T = [\mathbf{q}_u(t)^T, \mathbf{q}_v(t)^T, \mathbf{q}_w(t)^T]$ (the symbol $[\]$ indicates a row vector) as follows:

$$\begin{Bmatrix} u^0(x, y, t) \\ v^0(x, y, t) \\ w^0(x, y, t) \end{Bmatrix} = \begin{bmatrix} \mathbf{N}^u(x, y)^T & 0 & 0 \\ 0 & \mathbf{N}^v(x, y)^T & 0 \\ 0 & 0 & \mathbf{N}^w(x, y)^T \end{bmatrix} \begin{Bmatrix} \mathbf{q}_u(t) \\ \mathbf{q}_v(t) \\ \mathbf{q}_w(t) \end{Bmatrix}, \quad (5)$$

where $\mathbf{q}_u(t)$, $\mathbf{q}_v(t)$ are the vectors of generalised membrane displacements and $\mathbf{q}_w(t)$ is the vector generalised of transverse displacements. The matrix of shape functions $\mathbf{N}(x, y)$ is constituted by vectors of bi-dimensional membrane and transverse shape functions, which are, respectively, the following:

$$\mathbf{N}^u(x, y)^T = \mathbf{N}^v(x, y)^T = \{g_1(x)g_1(y), g_1(x)g_2(y), \dots, g_{p_i}(x)g_{p_i}(y)\}, \quad (6)$$

$$\mathbf{N}^w(x, y)^T = \{f_1(x)f_1(y), f_1(x)f_2(y), \dots, f_{p_0}(x)f_{p_0}(y)\}. \quad (7)$$

The vectors \mathbf{g} , \mathbf{f} , are the vectors of membrane and transverse, one-dimensional displacement shape functions; p_i and p_0 , are the numbers of g_i and f_i , respectively, displacement shape functions employed. In what concerns the transverse displacements, a set of hierarchic basis functions constituted by Legendre

polynomials in the Rodrigues’ form has been extensively applied [6,12–16] and will also be employed here. A set of polynomials called the g set, also used in Refs. [6,12–16] will be employed for the membrane displacements.

The geometrically non-linear strain–displacement relations are similar to the ones of Von Kármán for plates, but with additional terms to include the effects of the initial curvature

$$\begin{Bmatrix} \varepsilon_x \\ \varepsilon_y \\ \varepsilon_{xy} \end{Bmatrix} = \begin{Bmatrix} u_{,x}^0 + \frac{w^0}{R_1} + \frac{w_{,x}^{02}}{2} - zw_{,xx}^0 \\ v_{,y}^0 + \frac{w^0}{R_2} + \frac{w_{,y}^{02}}{2} - zw_{,yy}^0 \\ u_{,y}^0 + v_{,x}^0 + w_{,x}^0 w_{,y}^0 - 2zw_{,xy}^0 \end{Bmatrix}. \tag{8}$$

The constitutive equations for linear elastic isotropic materials are used.

The time domain equations of motion are derived by equating the sum of the virtual work of the inertia forces and of the elastic restoring forces to zero, as was done in Ref. [6]. These equations of motion have the following form:

$$\begin{bmatrix} \mathbf{M}_u^{11} & 0 & 0 \\ 0 & \mathbf{M}_v^{22} & 0 \\ 0 & 0 & \mathbf{M}_w^{33} \end{bmatrix} \begin{Bmatrix} \ddot{\mathbf{q}}_u(t) \\ \ddot{\mathbf{q}}_v(t) \\ \ddot{\mathbf{q}}_w(t) \end{Bmatrix} + \begin{bmatrix} \mathbf{KL}_u^{11} & 0 & \mathbf{KL}_{us}^{13} \\ 0 & \mathbf{KL}_v^{22} & \mathbf{KL}_{vs}^{23} \\ \mathbf{KL}_{su}^{31} & \mathbf{KL}_{sv}^{32} & \mathbf{KL}_{ss}^{33} + \mathbf{KL}_b^{33} \end{bmatrix} \begin{Bmatrix} \mathbf{q}_u(t) \\ \mathbf{q}_v(t) \\ \mathbf{q}_w(t) \end{Bmatrix} + \begin{bmatrix} 0 & 0 & \mathbf{KNL}_2^{13} \\ 0 & 0 & \mathbf{KNL}_2^{23} \\ 2\mathbf{KNL}_2^{13T} & 2\mathbf{KNL}_2^{23T} & \mathbf{KNL}_4^{33} + \mathbf{KNL}_{2s}^{33} + 2\mathbf{KNL}_{2s}^{33T} \end{bmatrix} \begin{Bmatrix} \mathbf{q}_u(t) \\ \mathbf{q}_v(t) \\ \mathbf{q}_w(t) \end{Bmatrix} = \begin{Bmatrix} 0 \\ 0 \\ 0 \end{Bmatrix}. \tag{9}$$

Matrices \mathbf{M}_u^{11} and \mathbf{M}_v^{22} are the membrane inertia matrices and matrix \mathbf{M}_w^{33} is the transverse inertia matrix. Matrices of type \mathbf{KL}_k^{ij} are constant stiffness matrices; in particular, matrices \mathbf{KL}_u^{11} and \mathbf{KL}_v^{22} are membrane stiffness matrices, matrix \mathbf{KL}_b^{33} is the bending stiffness matrix; matrices \mathbf{KL}_{us}^{13} , \mathbf{KL}_{vs}^{23} and \mathbf{KL}_{sv}^{32} are due to coupling between the transverse deflection and the membrane deflection, which occurs because of the shell curvature; matrix \mathbf{KL}_{ss}^{33} is due to the transverse deflection and to the shell curvature. There are four stiffness matrices that depend on the generalised transverse displacements \mathbf{q}_w , originating non-linear terms. These are the matrices \mathbf{KNL}_2^{i3} , $i = 1, 2$, and \mathbf{KNL}_{2s}^{33} which depend linearly on \mathbf{q}_w , and matrix \mathbf{KNL}_4^{33} , which is a quadratic function of \mathbf{q}_w . It is pointed out that a more correct notation of all terms that depend on $\mathbf{q}_w(t)$, as for example \mathbf{KNL}_2^{13} , would be $\mathbf{KNL}_2^{13}(\mathbf{q}_w(t))$, but this notation was not used for the sakes of simplicity and readability (actually, for the same reason $\mathbf{q}_w(t)$ is sometimes written simply as \mathbf{q}_w , etc.).

When the boundaries are fixed, the middle surface membrane displacements are smaller than the transverse displacements, particularly if the shell is not deep. It is widely accepted that in thin plates the membrane inertia may in most cases be neglected with a small accuracy loss. However, it is debatable whether the membrane inertia of shallow shells can be neglected or not [1,7]. Only shallow shells with immovable clamped boundaries will be analysed and a few numerical tests carried out in the time domain indicated that it is reasonable to neglect membrane inertia in this case. This approach will be partially validated in Section 3.2 by computing the natural frequencies using models with and without membrane inertia.

Neglecting the membrane inertia and using Eq. (9), the generalised membrane displacements are expressed as

$$\begin{aligned} \mathbf{q}_u(t) &= -\mathbf{KL}_u^{11-1} (\mathbf{KL}_{us}^{13} + \mathbf{KNL}_2^{13}) \mathbf{q}_w(t), \\ \mathbf{q}_v(t) &= -\mathbf{KL}_v^{22-1} (\mathbf{KL}_{vs}^{23} + \mathbf{KNL}_2^{23}) \mathbf{q}_w(t). \end{aligned} \tag{10}$$

Thus, the following condensed time domain equations of motion are obtained:

$$\begin{aligned} \mathbf{M}_w^{33} \ddot{\mathbf{q}}_w(t) + & \left[\mathbf{K}L_{ss}^{33} + \mathbf{K}L_b^{33} - \mathbf{K}L_{su}^{13} \mathbf{K}L_u^{11^{-1}} \mathbf{K}L_{us}^{13} - \mathbf{K}L_{sv}^{32} \mathbf{K}L_v^{22^{-1}} \mathbf{K}L_{vs}^{23} \right] \mathbf{q}_w(t) \\ & + \left[\mathbf{K}N L_{2s}^{33} + 2\mathbf{K}N L_{2s}^{33T} - \mathbf{K}L_{su}^{31} \mathbf{K}L_u^{11^{-1}} \mathbf{K}N L_2^{13} - \mathbf{K}L_{sv}^{32} \mathbf{K}L_v^{22^{-1}} \mathbf{K}N L_2^{23} - 2\mathbf{K}N L_2^{13T} \mathbf{K}L_u^{11^{-1}} \mathbf{K}L_{us}^{13} \right. \\ & \left. - 2\mathbf{K}N L_2^{23T} \mathbf{K}L_v^{22^{-1}} \mathbf{K}L_{vs}^{23} \right] \mathbf{q}_w(t) + \left[\mathbf{K}N L_4^{33} - 2\mathbf{K}N L_2^{13T} \mathbf{K}L_u^{11^{-1}} \mathbf{K}N L_2^{13} - 2\mathbf{K}N L_2^{23T} \mathbf{K}L_v^{11^{-1}} \mathbf{K}N L_2^{23} \right] \\ & \times \mathbf{q}_w(t) = 0. \end{aligned} \quad (11)$$

The number of degrees of freedom in Eq. (11) is $n = p_o^2$. Although the model above requires a moderate number of degrees of freedom for accuracy, this number will be further reduced by applying a standard modal condensation procedure. To this effect, the linear modes of vibration are computed solving the eigenvalue problem:

$$\left(\left[\mathbf{K}L_{ss}^{33} + \mathbf{K}L_b^{33} - \mathbf{K}L_{su}^{31} \mathbf{K}L_u^{11^{-1}} \mathbf{K}L_{us}^{13} - \mathbf{K}L_{sv}^{32} - \mathbf{K}L_v^{22^{-1}} \mathbf{K}L_{vs}^{23} \right] - \omega^2 \mathbf{M}_w^{23} \right) \boldsymbol{\phi} = \mathbf{0} \quad (12)$$

and a rectangular matrix $\boldsymbol{\Phi}_{n \times m}$, whose columns are vectors that represent the first m linear mode shapes, is defined. The equations of motion are transformed into a reduced set of m equations in modal coordinates \mathbf{q}_m , as follows:

$$\mathbf{q}_w(t) \cong \boldsymbol{\Phi}_{n \times m} \mathbf{q}_m(t), \quad (13)$$

$$\begin{aligned} \boldsymbol{\Phi}^T \mathbf{M}_w^{33} \boldsymbol{\Phi} \ddot{\mathbf{q}}_m(t) + \boldsymbol{\Phi}^T \left[\mathbf{K}L_{ss}^{33} + \mathbf{K}L_b^{33} - \mathbf{K}L_{su}^{31} \mathbf{K}L_{su}^{31^{-1}} \mathbf{K}L_{us}^{13} - \mathbf{K}L_{sv}^{32} \mathbf{K}L_v^{22^{-1}} \mathbf{K}L_{vs}^{23} \right] \boldsymbol{\Phi} \mathbf{q}_m(t) \\ + \boldsymbol{\Phi}^T \left[\mathbf{K}N L_{2s}^{33} + 2\mathbf{K}N L_{2s}^{33T} - \mathbf{K}L_{su}^{31} \mathbf{K}L_u^{11^{-1}} \mathbf{K}N L_2^{13} - \mathbf{K}L_{sv}^{32} \mathbf{K}L_v^{22^{-1}} \mathbf{K}N L_2^{23} - 2\mathbf{K}N L_2^{13T} \mathbf{K}L_u^{11^{-1}} \mathbf{K}L_{us}^{13} \right. \\ \left. - 2\mathbf{K}N L_2^{23T} \mathbf{K}L_v^{22^{-1}} \mathbf{K}L_{vs}^{23} \right] \boldsymbol{\Phi} \mathbf{q}_m(t) + \boldsymbol{\Phi}^T \left[\mathbf{K}N L_4^{33} - 2\mathbf{K}N L_2^{13T} \mathbf{K}L_u^{11^{-1}} \mathbf{K}N L_2^{13} - 2\mathbf{K}N L_2^{23T} \mathbf{K}L_v^{11^{-1}} \mathbf{K}N L_2^{23} \right] \\ \times \boldsymbol{\Phi} \mathbf{q}_m(t) = 0, \\ \Leftrightarrow \mathbf{M} \ddot{\mathbf{q}}_m(t) + \mathbf{K} \mathbf{q}_m(t) + \mathbf{K}n \mathbf{q}_m(t) = 0, \end{aligned} \quad (14)$$

The harmonic balance method is now applied in order to obtain a set of algebraic equations which depend on the fundamental frequency of vibration and on the coefficients of each harmonic. An appropriate choice of the number of harmonics in the truncated Fourier series is important: it should not be so small that it introduces errors or so large that it leads to unnecessary and cumbersome algebraic derivations. In the choice of truncated Fourier series, it should be taken into account that only undamped periodic motions will be analysed and that quadratic and cubic non-linear terms are present in the equations of motion (14). The latter condition advises one to consider the constant term, odd and even harmonics in the Fourier series (15); the former implies that sine terms are not necessary. A large number of numerical tests employing numerical integration of the equations of motion in the time domain were carried out; some of these tests are shown in Ref. [17]. Spectra of the time domain responses were obtained and, although in a limited number of tests higher order harmonics appeared, in the majority of cases the constant term and the first three harmonics were the only significant ones. Consequently, the modal coordinates will be expressed as

$$\mathbf{q}_m(t) = \frac{1}{2} \mathbf{w}_{c0} + \sum_{i=1}^k \mathbf{w}_{ci} \cos(i\omega t) \quad (15)$$

and k will be made equal to three. Inserting the truncated series (15) into Eq. (14) and applying the harmonic balance method, one obtains a set of algebraic equations which depend on the fundamental frequency of

vibration and on the coefficients of each harmonic:

$$\left(-\omega^2 \begin{bmatrix} 0 & 0 & 0 & 0 \\ 0 & \mathbf{M} & 0 & 0 \\ 0 & 0 & 4\mathbf{M} & 0 \\ 0 & 0 & 0 & 9\mathbf{M} \end{bmatrix} + \begin{bmatrix} \frac{1}{2}\mathbf{K}l & 0 & 0 & 0 \\ 0 & \mathbf{K}l & 0 & 0 \\ 0 & 0 & \mathbf{K}l & 0 \\ 0 & 0 & 0 & \mathbf{K}l \end{bmatrix} \right) \begin{Bmatrix} \mathbf{w}_{c0} \\ \mathbf{w}_{c1} \\ \mathbf{w}_{c2} \\ \mathbf{w}_{c3} \end{Bmatrix} + \begin{Bmatrix} \mathbf{F}_{c0} \\ \mathbf{F}_{c1} \\ \mathbf{F}_{c2} \\ \mathbf{F}_{c3} \end{Bmatrix} = \begin{Bmatrix} 0 \\ 0 \\ 0 \\ 0 \end{Bmatrix}. \tag{16}$$

Eq. (16) can also be understood as frequency domain equations of motion. The coefficients of the harmonics form a vector $\mathbf{w}_C^T = \{\mathbf{w}_{c0}, \mathbf{w}_{c1}, \mathbf{w}_{c2}, \mathbf{w}_{c3}\}^T$. The vector $\mathbf{q}_m(t)$ is an even function of time and the non-linear terms— $\mathbf{F}_{c0}, \mathbf{F}_{c1}, \mathbf{F}_{c2}$, and \mathbf{F}_{c3} —are defined by

$$\mathbf{F}_{ci} = \frac{2}{T} \int_0^T \mathbf{K}nl \mathbf{q}_m(t) \cos(i\omega t) dt, \quad i = 0, 1, 2, 3. \tag{17}$$

The application of Eqs. (16) and (17) is equivalent to select the coefficients of each harmonic.

Solving Eq. (16) is equivalent to find the vector $\mathbf{w}_C^T = \{\mathbf{w}_{c0}, \mathbf{w}_{c1}, \mathbf{w}_{c2}, \mathbf{w}_{c3}\}^T$ and the frequency ω^2 , that make the following vector \mathbf{F} equal to the null vector:

$$\mathbf{F} = \left(-\omega^2 \begin{bmatrix} 0 & 0 & 0 & 0 \\ 0 & \mathbf{M} & 0 & 0 \\ 0 & 0 & 4\mathbf{M} & 0 \\ 0 & 0 & 0 & 9\mathbf{M} \end{bmatrix} + \begin{bmatrix} \frac{1}{2}\mathbf{K}l & 0 & 0 & 0 \\ 0 & \mathbf{K}l & 0 & 0 \\ 0 & 0 & \mathbf{K}l & 0 \\ 0 & 0 & 0 & \mathbf{K}l \end{bmatrix} \right) \begin{Bmatrix} \mathbf{w}_{c0} \\ \mathbf{w}_{c1} \\ \mathbf{w}_{c2} \\ \mathbf{w}_{c3} \end{Bmatrix} + \begin{Bmatrix} \mathbf{F}_{c0} \\ \mathbf{F}_{c1} \\ \mathbf{F}_{c2} \\ \mathbf{F}_{c3} \end{Bmatrix}. \tag{18}$$

This is an eigenvalue problem where one of the matrices depends on the eigenvector, a problem that may be solved by an arc-length continuation method [14,20]. This method is essentially a Newton–Raphson procedure, but instead of using the frequency or the amplitude of vibration as a parameter, the distance between two points of the backbone curve is employed, which allows one to pass turning points. In each step, both ω and \mathbf{w}_C are not know.

Solving Eq. (18) frequency and shapes of vibration that depend on the amplitude of vibration displacement are obtained. We say that the pair frequency/mode shape represents a non-linear mode of vibration of the undamped shell. In what concerns the shapes of vibration, one can distinguish three cases. The first one—that was not found here in the numerical applications, but was found before in plates [15]—is the case where there is no internal resonance and only one vector $\mathbf{w}_{ci}, i = 1, 2, 3, 4$, is different from zero. In this case, we would have obtained an approximation to the true non-linear mode shape, but where, unlike what happens in reality, the shape does not change during a given motion. In the second case, found in the numerical applications shown here, there is still no internal resonance, but at least two $\mathbf{w}_{ci}, i = 1,2,3,4$ are different from zero. It is easy to see from Eq. (15) that in this case the present model results in a (non-linear mode) shape that changes during a specified motion: it is not “self-similar at all times” [21]. Finally, we have the case of internal resonance where two modes are coupled [22].

It is recalled that there is a number of publications on the variation of mode shapes with amplitude, as for example the influential Refs. [23,24]. Moreover, the so-called “non-linear normal modes” gave rise to a number of publications after important works like [25,26]. Clearly, the approach followed in this paper uses iterative methods and does not provide expressions for the non-linear modes that one can use in model reduction.

3. Numerical results and discussions

3.1. Validation

Partial validation of the approach here developed was conducted by comparing the linear and non-linear natural frequencies of the present model with results obtained by other authors. In Table 1 frequency

Table 1

First four-frequency parameters of a completely free cylindrical shell ($a/h = 100$, $a/b = 1$, $R_1/a = 2$, $R_2 = \infty$, $\nu = 0.3$)

References	Mode number			
	1	2	3	4
Ribeiro, <i>p</i> -version FSDT [16]	13.466	22.063	34.767	48.596
Bardell et al., [27] Ansys 100×100	13.403	21.473	34.148	48.913
Bardell et al. [27] HFEM, $p_o = p_i = 10$	13.403	21.473	34.147	48.908
Leissa and Narita [28]	13.508	22.073	34.868	48.703
Present, $p_o = p_i = 10$	13.508	22.072	34.868	48.703

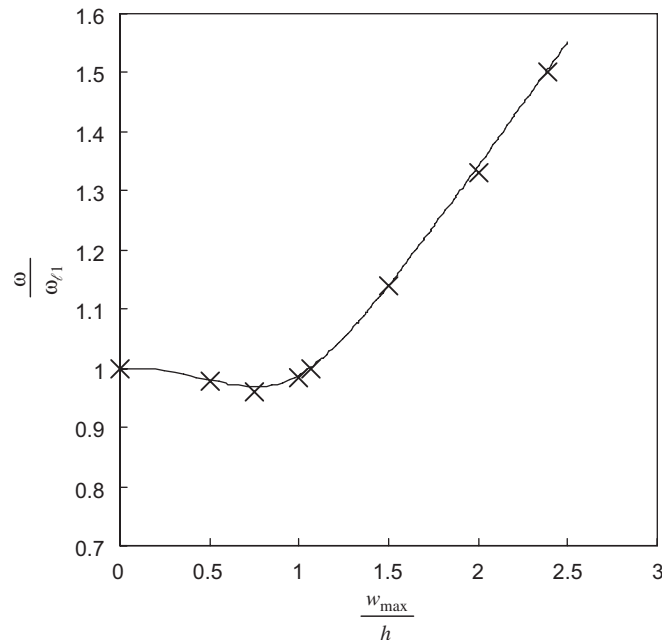


Fig. 2. Non-linear natural frequency versus amplitude for a cylindrical shell: —, present solution; ×, solutions from Ref. [3].

parameters in the linear regime are given; the parameters are defined as $\Omega = \omega b^2 \sqrt{\rho h/D}$, where D is the flexural rigidity, $Eh^3/(12(1 - \nu^2))$. The present code gives similar values to the ones published.

Proceeding to the non-linear regime, a comparison is carried out with Kobayashi and Leissa [3] and with Przekop et al. [7]. The case study is a cylindrical shell supported by shear diaphragms, such that the boundary conditions for a thin shell are the following:

$$v^0(x, y, t) = w^0(x, y, t) = 0, w^0_{,y}(x, y, t) = 0, N_x(x, y, t) = 0, M_x(x, y, t) = 0 \text{ at } x = \pm \frac{a}{2},$$

$$u^0(x, y, t) = w^0(x, y, t) = 0, w^0_{,x}(x, y, t) = 0, N_y(x, y, t) = 0, M_y(x, y, t) = 0 \text{ at } y = \pm \frac{b}{2}.$$

The geometric characteristics respect the following relations: $R_x/a = 0.1$, $h/a = 0.01$, $b/a = 1$; and the Poisson coefficient is $\nu = 0.3$. Fig. 2 presents the frequency ratio ω/ω_{l1} —where ω_{l1} represents the natural frequency of the first bi-symmetric linear mode—in function of the non-dimensional maximum positive deflection w_{max}/h for a cylindrical shallow shell. A single mode model was employed, as in Refs. [3,7], and the values here obtained agree with the ones given in Ref. [3]. Visual comparison with the figure given in Ref. [7] also indicates close agreement.

Table 2
Shells curvature radius and thickness

	Shell 1	Shell 2	Shell 3	Shell 4
Curvature radius	$b/R = 0.4$	$b/R = 0.2$	$b/R = 0.4$	$b/R = 0.2$
Thickness (m)	$h = 0.001$	$h = 0.001$	$h = 0.0025$	$h = 0.0025$

Table 3
Convergence of linear natural frequencies (rad/s) of Shell 1, bi-symmetric modes

Mode	Number of shape functions					
	$p_o = 6, p_i = 10^a$	$p_o = 6, p_i = 10^b$	$p_o = 6, p_i = 12^a$	$p_o = 6, p_i = 12^b$	$p_o = 8, p_i = 14^a$	$p_o = 8, p_i = 14^b$
1	1138.96	1137.62	1138.95	1137.61	1138.95	1137.61
2	1914.86	1913.62	1911.35	1910.12	1911.28	1910.05
3	2476.97	2475.86	2476.54	2475.43	2476.53	2475.42
4	2966.94	2965.53	2961.28	2959.88	2961.08	2959.68
5	3480.34	3479.20	3353.24	3352.12	3337.79	3336.69
6	3817.94	3817.08	3814.89	3814.02	3814.64	3813.78
7	3875.83	3875.11	3840.06	3839.27	3835.50	3834.71
8	4147.45	4146.71	4140.24	4139.58	4130.22	4129.80
9	4254.13	4253.82	4160.89	4160.48	4148.35	4147.69
10	4398.28	4397.97	4335.39	4334.86	4313.98	4313.44
11	4504.96	4504.34	4412.67	4412.33	4408.70	4408.37
12	5295.77	5295.57	5241.97	5241.60	5225.68	5225.29

^aWithout membrane inertia.

^bWith membrane inertia.

3.2. Properties of shells and analyses of convergence

Four panels will be now studied, in order to analyse the variation of the non-linear natural frequencies with the initial curvature radius and thickness, properties given in Table 2. The relation between the curvature and the projected length is within the accepted limit for a shell to be considered shallow, which is either 0.4 or 0.5, depending on the source [1,19,28]. The ratio between the thickness and the projected length is either $h/b = 0.002$ or 0.005 , i.e., the shells are very thin so that thin shell theory applies even if high-order modes are present in the motion. The material properties are $E = 7 \times 10^{10} \text{ N/m}^2$, $\rho = 2778 \text{ kg/m}^3$ and $\nu = 0.33$, which are typical properties of aluminium. E is the Young modulus, ρ the mass density and ν the Poisson ratio. The shells have quadrangular planform ($a = b$), with side length equal to 0.5 m and are fully clamped.

The designation “main branch” is used for a branch of periodic free vibration solutions, which starts at zero vibration amplitude and either at a linear natural frequency or at a linear natural frequency divided by an integer. The continuation method will be started at the first bi-symmetric (i.e. symmetric with respect to planes xz and yz) linear mode. Using models with symmetric and antisymmetric transverse shape functions to carry out preliminary analyses of Shells 1–4, only bi-symmetric transverse modes were found in this main branch of solutions. This behaviour is similar to the one encountered in plates [15], where coupling between symmetric and antisymmetric modes only occurred in bifurcated branches. Taking those numerical experiences as a valid indication, the models employed in the analyses that follow only contain symmetric f functions. Both symmetric and antisymmetric g shape functions are still required for the membrane displacements.

The third harmonic is the highest harmonic present in the Fourier expansion (15) of the generalised coordinates and a hardening spring effect may occur. If we intend to study the periodic vibrations until a fundamental non-linear frequency equal to $1.25\omega_{\ell 1}$, then all the linear modes with natural frequencies smaller than $1.25 \times 3 \times \omega_{\ell 1}$ should be included in the model and these modes ought to be computed with reasonable accuracy. Tables 3–6 show the linear natural frequencies computed with various models, either full (eigenvalue problem that results from Eq. (9) without non-linear terms) or reduced by neglecting the membrane inertia,

Table 4
Convergence of linear natural frequencies (rad/s) of Shell 2, bi-symmetric modes

Mode	Number of shape functions					
	$p_o = 6, p_i = 10^a$	$p_o = 6, p_i = 10^b$	$p_o = 6, p_i = 12^a$	$p_o = 6, p_i = 12^b$	$p_o = 8, p_i = 14^a$	$p_o = 8, p_i = 14^b$
1	865.639	865.36	865.64	865.359	865.638	865.359
2	1722.83	1722.60	1722.46	1722.228	1722.453	1722.222
3	1749.72	1749.47	1749.71	1749.46	1749.71	1749.46
4	2073.23	2073.13	2073.15	2073.05	2073.15	2073.04
5	2170.26	2170.20	2168.78	2168.71	2168.72	2168.65
6	2579.44	2579.26	2578.31	2578.13	2578.27	2578.09
7	2711.99	2711.92	2711.49	2711.42	2711.47	2711.40
8	2878.58	2878.45	2877.65	2877.52	2877.62	2877.49
9	3587.97	3587.76	3521.59	3521.36	3502.15	3501.93
10	3644.18	3644.00	3642.97	3642.80	3642.92	3642.75
11	4019.62	4019.58	4007.94	4007.90	3993.34	3993.30
12	4098.92	4098.74	4043.57	4043.36	4026.84	4026.64

^aWithout membrane inertia.

^bWith membrane inertia.

Table 5
Convergence of linear natural frequencies (rad/s) of Shell 3, bi-symmetric modes

Mode	Number of shape functions					
	$p_o = 6, p_i = 10^a$	$p_o = 6, p_i = 10^b$	$p_o = 6, p_i = 12^a$	$p_o = 6, p_i = 12^b$	$p_o = 8, p_i = 14^a$	$p_o = 8, p_i = 14^b$
1	2047.66	2044.98	2047.66	2044.97	2047.66	2044.97
2	3782.53	3781.28	3782.43	3781.18	3782.43	3781.18
3	3960.62	3958.38	3960.62	3958.38	3960.62	3958.37
4	4450.55	4449.73	4450.53	4449.72	4450.53	4449.72
5	4994.35	4992.90	4991.79	4990.33	4991.69	4990.24
6	6129.77	6129.18	6129.04	6128.45	6128.99	6128.40
7	6283.29	6281.37	6281.61	6279.69	6281.55	6279.62
8	6799.69	6798.40	6797.95	6796.65	6797.88	6796.59
9	8877.80	8875.62	8767.85	8765.53	8722.48	8720.21
10	8937.86	8936.12	8935.82	8934.08	8935.70	8933.96
11	9592.47	9592.15	9573.50	9573.13	9535.98	9535.61
12	10151.3	10149.4	10059.8	10057.7	10021.0	10019.0

^aWithout membrane inertia.

^bWith membrane inertia.

Eq. (12). Rather accurate values are obtained with the $p_o = 6, p_i = 10$ models without membrane inertia, and these will be the original models employed. In what concerns the modal reduction, we can see that 10 modes of Shell 1 have frequencies lower than $1.25 \times 3 \times \omega_{r1}$: 10 linear modes are used in the modal reduction. In the other shells not so many modes would be required, but 10 modes will also be employed.

3.3. Backbone curves and shapes of vibration

To define the backbone curves, the amplitude of the i th harmonic at point (x_p, y_p) is computed as

$$\mathbf{w}_i = \mathbf{N}_w(x_p, y_p)_n^T \mathbf{\Phi}_{n \times m} \mathbf{w}_{cim}. \quad (19)$$

Table 6
Convergence of linear natural frequencies (rad/s) of Shell 4, bi-symmetric modes

Mode	Number of shape functions					
	$p_o = 6, p_i = 10^a$	$p_o = 6, p_i = 10^b$	$p_o = 6, p_i = 12^a$	$p_o = 6, p_i = 12^b$	$p_o = 8, p_i = 14^a$	$p_o = 8, p_i = 14^b$
1	1663.23	1662.75	1663.23	1662.75	1663.23	1662.75
2	2337.87	2337.67	2337.87	2337.67	2337.87	2337.67
3	2759.03	2758.85	2759.02	2758.85	2759.02	2758.85
4	3603.74	3603.32	3603.74	3603.32	3603.74	3603.31
5	4778.28	4777.75	4777.68	4777.15	4777.62	4777.10
6	5128.63	5128.53	5128.43	5128.33	5128.39	5128.29
7	6093.91	6093.41	6093.52	6093.02	6093.48	6092.98
8	6237.83	6237.52	6237.31	6237.00	6237.27	6236.96
9	8706.60	8706.17	8705.90	8705.47	8688.80	8688.22
10	8759.54	8758.99	8730.92	8730.33	8706.66	8706.22
11	8946.33	8946.25	8941.27	8941.19	8902.02	8901.93
12	10023.5	10023.1	9999.83	9999.31	9964.85	9964.33

^aWithout membrane inertia.

^bWith membrane inertia.

W_0 is additionally multiplied by $\frac{1}{2}$ so that it represents the offset of $w^0(x, y, t)$ from zero (see Eq. (15)). The displacement with respect to the reference plate, $w^i(x, y)$ which is given by Eq. (1), is neither included in the representation of W_0 nor in the sections of mode shapes shown later.

Fig. 3 shows the backbone curves of Shell 1, which were traced by starting the continuation method at the first linear bi-symmetric mode of vibration ($\omega/\omega_{\ell 1} = 1$, near zero vibration amplitude). There is a softening spring effect from the linear solution until $\omega/\omega_{\ell 1} \approx 0.95$, accompanied by a visible increase of the absolute amplitudes at $(x, y) = (0, 0)$ of all harmonics except the second, which is almost zero. The first harmonic dominates in this region. At $\omega/\omega_{\ell 1} \approx 0.95$ there is a singular point [29], followed by a hardening spring effect, where, at $(x, y) = (0, 0)$, the amplitudes of the constant term, first harmonic and second harmonic slightly increase and the third harmonic markedly increases; more singular points occur after. The constant term and the three harmonics considered in the series are, in different proportions, present in all solutions.

It is advisable to compute the backbone curve at another location, because, as shown in the appendix, some modes have low vibration amplitude at $(0, 0)$. Hence, the backbone curve was also computed at $(x, y) = (0, b/3)$. Fig. 4 shows that the second harmonic is rather meaningful also in the range of frequencies $0.95 < \omega/\omega_{\ell 1} < 1$.

It is also very informative to plot the shapes assumed by the different harmonics. In Fig. 5 we can see some sections of these shapes at particular points of the backbone curve, points which are defined by the non-linear frequencies of vibration and vibration amplitudes. These sections were defined using Eq. (19), but with $x_p = 0$ and y_p varying from 0 to $b/2$. Furthermore, the sections were normalised such that the amplitude is equal to one at point $(x, y) = (0, 0)$ or at the point of maximum amplitude displacement in the sole case of the second harmonic. The amplitudes of displacement achieved by each harmonic at $(x, y) = (0, 0)$ are given in the figure legend.

In conclusion, analysing the ensemble of computed data one finds out that from $\omega/\omega_{\ell 1} = 1$ to $\approx .95$ the shell experiences oscillations where the first harmonic dominates, with a shape that is similar, but not equal, to the first linear mode (it is stressed that this shape changes both with the maximum vibration amplitude and during the period of oscillation). The singular point at $\omega/\omega_{\ell 1} \approx .95$ is due to the transfer of energy to higher order modes of vibration, which are connected with the second and third harmonics. The second harmonic becomes at this stage dominated by the second mode, but other modal coordinates appear, which is understandable because the second non-linear mode is different from the linear one. Interaction between modes also occurs at other points (for example at solutions with a dimensional frequency $\omega/\omega_{\ell 1} \approx 1$, but finite

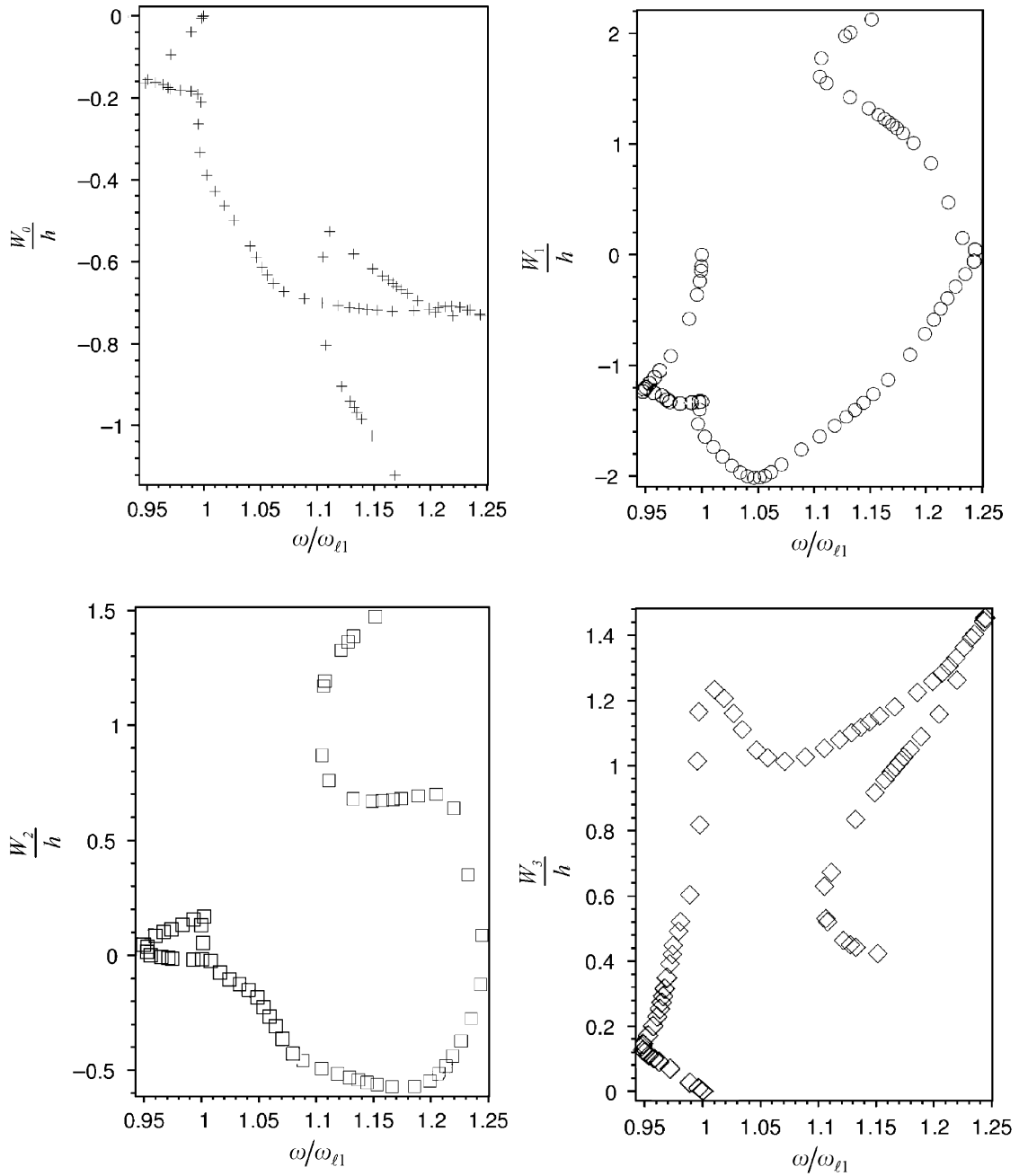


Fig. 3. Backbone curve of Shell 1 ($a/h = 500$, $a/b = 1$, $b/R = 0.4$) at $(x, y) = (0, 0)$: +, constant term; \circ , first harmonic; \square , second harmonic; \diamond , third harmonic.

amplitude of vibration, and at $\omega/\omega_{l1} \approx 1.11$), causing the amplitudes of each harmonic to increase or decrease as modes gain or lose influence.

It is noticeable that the backbone curve is more complex than any of the backbones found in plates in former studies, Ref. [15], and that the number of interactions detected between modes in a short frequency span is greater in shells than in plates (please note that even more solutions could be found here, had we included antisymmetric functions and explored all bifurcation points). This behaviour is explained by the

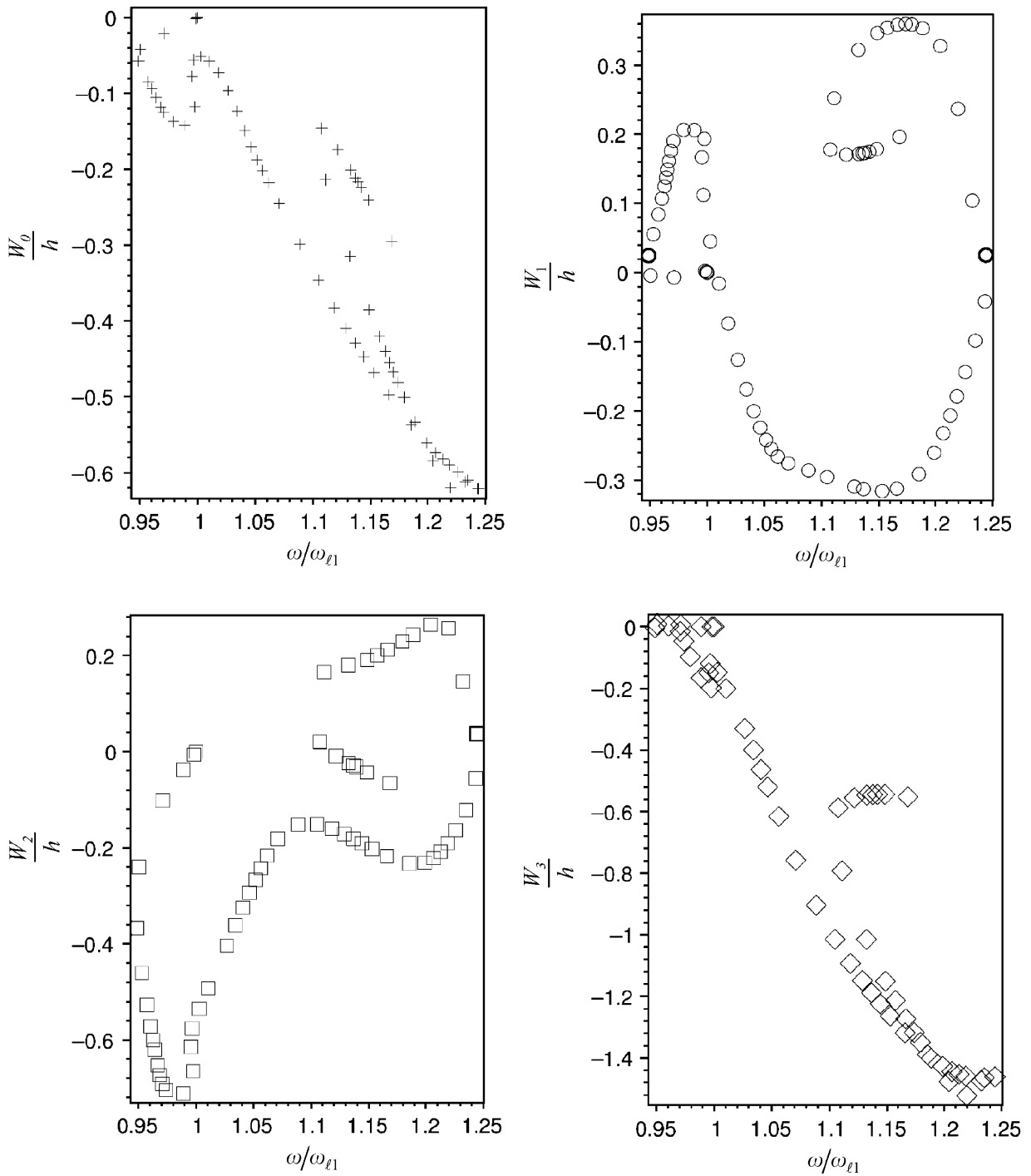


Fig. 4. Backbone curve of Shell 1 ($a/h = 500$, $a/b = 1$, $b/R = 0.4$) at $(x, y) = (0, b/3)$: +, constant term; o, first harmonic; square, second harmonic; diamond, third harmonic.

quadratic and cubic terms that appear in the condensed equations of motion of shallow shells—the condensed equations of plates only have cubic non-linear terms—and by the stronger relation between membrane and transverse displacements in the case of shells.

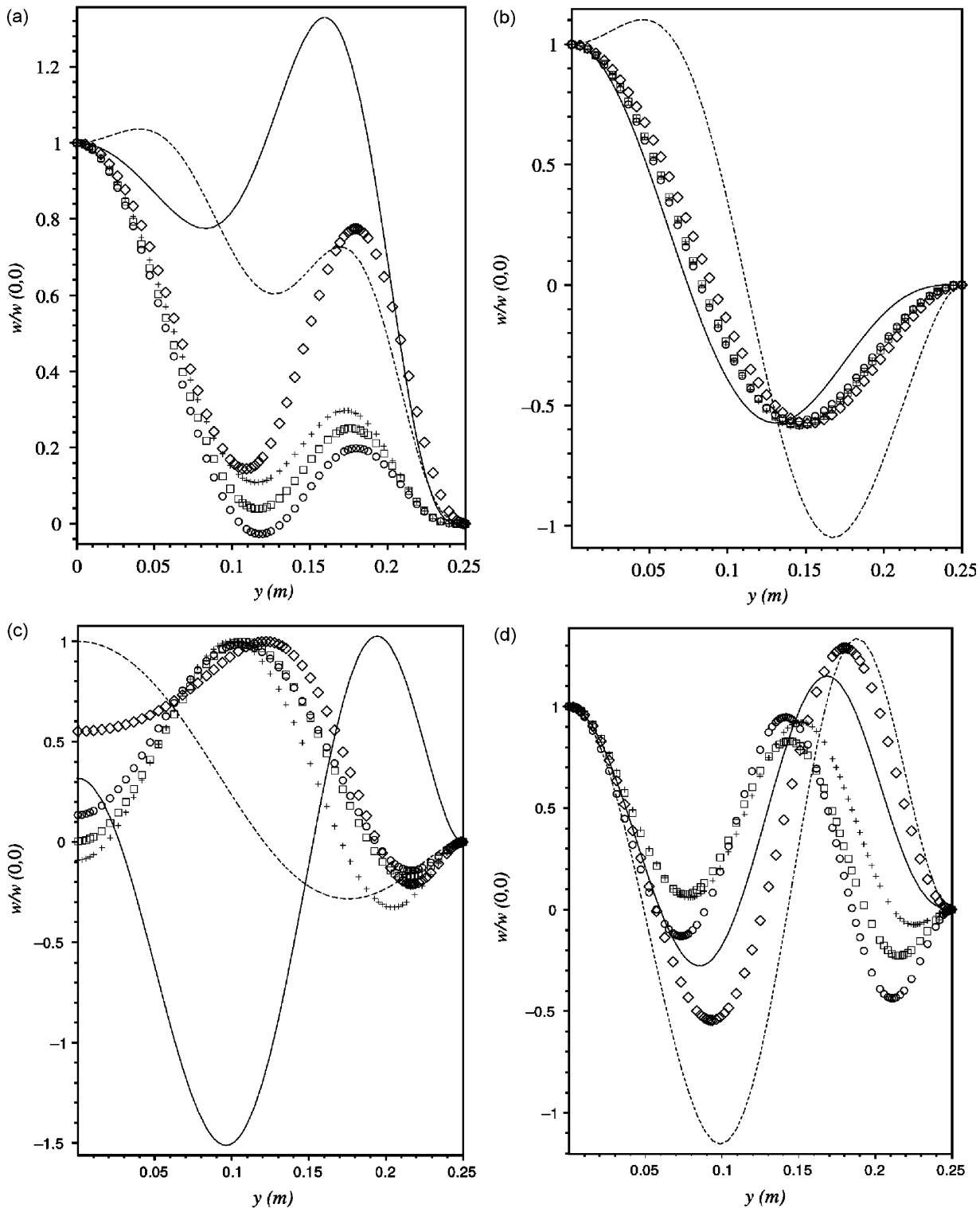


Fig. 5. Sections, $x = 0$, of normalised shapes of Shell 1: (a) constant term, (b) first harmonic, (c) second harmonic, (d) third harmonic: \circ , $\omega/\omega_{r1} \approx 1$ and $W_0/h = -1.3 \times 10^{-3}$, $W_1/h = -0.104$, $W_2/h = -1.75 \times 10^{-4}$, $W_3/h = 2.45 \times 10^{-2}$; \square , $\omega/\omega_{r1} = 0.97$ and $W_0/h = -9.5 \times 10^{-2}$, $W_1/h = -0.926$, $W_2/h = -3.62 \times 10^{-4}$, $W_3/h = 6.52 \times 10^{-2}$; $+$, $\omega/\omega_{r1} = .95$ and $W_0/h = -.155$, $W_1/h = -1.20$, $W_2/h = 2.36 \times 10^{-2}$, $W_3/h = 0.113$; $-$, $\omega/\omega_{r1} = .989$ and $W_0/h = -.184$, $W_1/h = -1.33$, $W_2/h = 0.158$, $W_3/h = 0.604$; \diamond , $\omega/\omega_{r1} = 1.05$ and $W_0/h = -0.589$, $W_1/h = -2.014$, $W_2/h = -0.196$, $W_3/h = 1.047$; $- -$, $\omega/\omega_{r1} = 1.24$ and $W_0/h = -0.730$, $W_1/h = 3.41 \times 10^{-2}$, $W_2/h = 8.62 \times 10^{-2}$, $W_3/h = 1.45$.

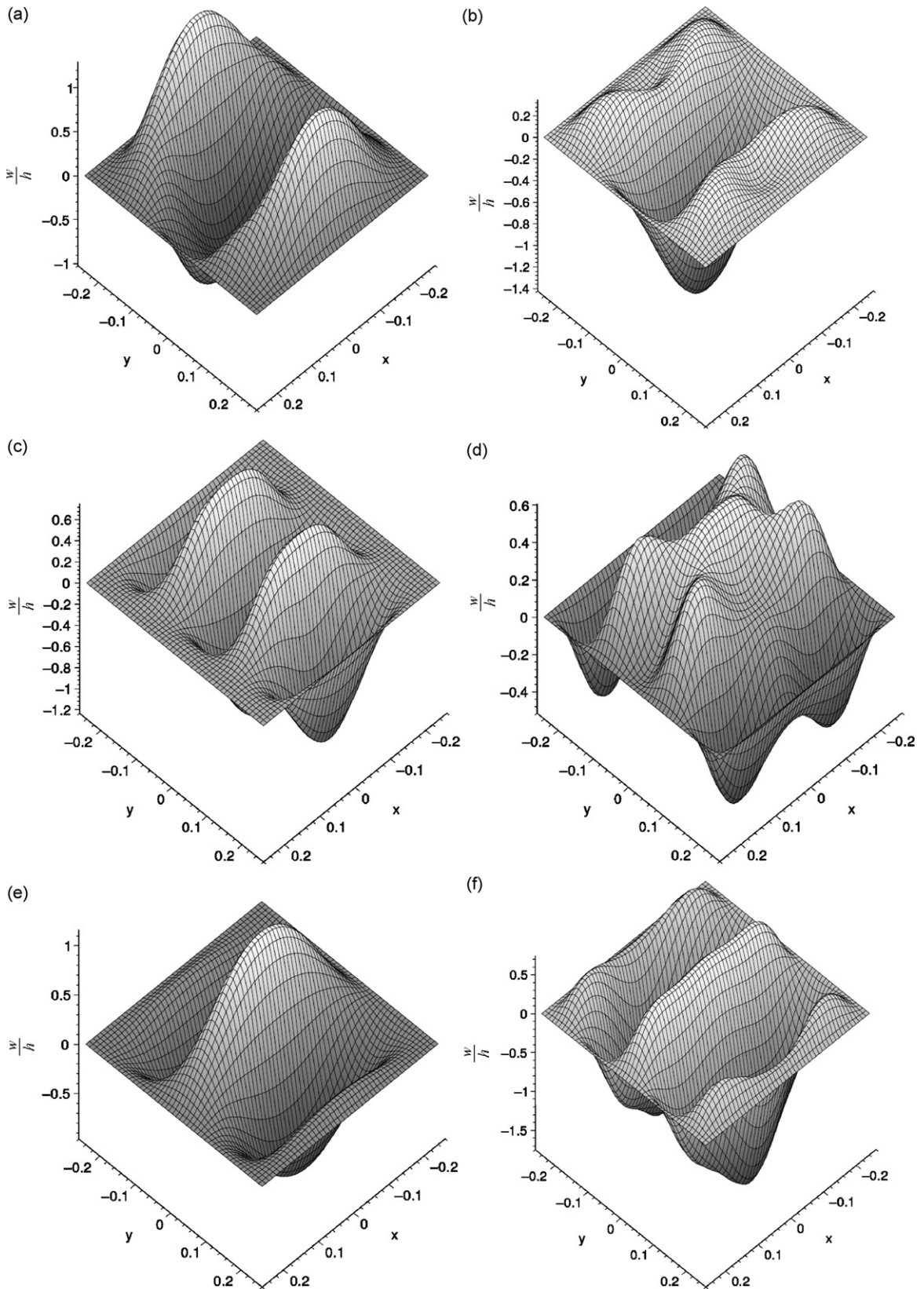


Fig. 6. Shapes of Shell 1 when $\omega/\omega_{r1} = 0.989$, at different instants: (a) $t = 0$, (b) $t = T/10$, (c) $t = T/5$, (d) $t = 3T/10$, (e) $t = 4T/10$ and (f) $t = T/2$.

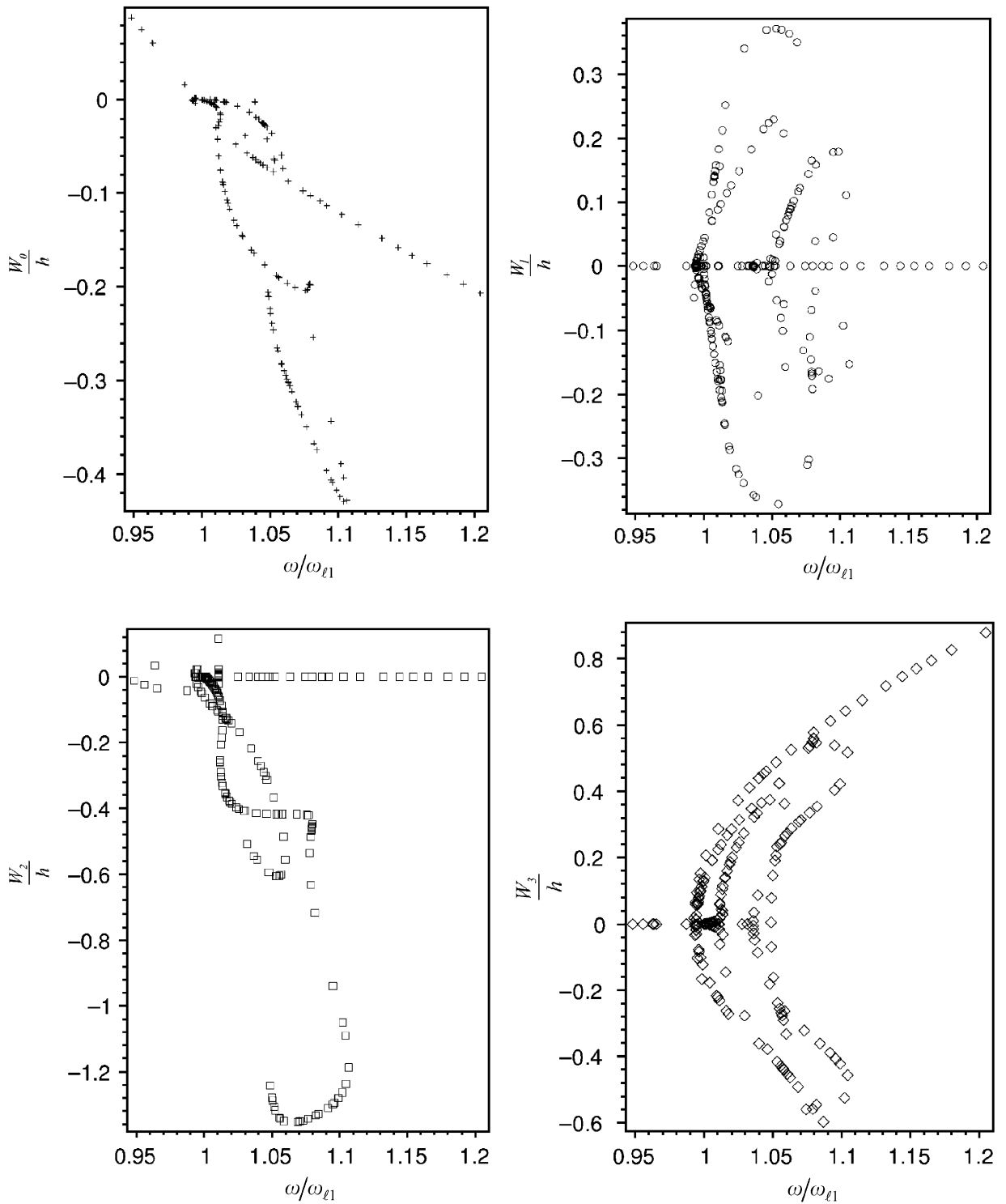


Fig. 7. Backbone curve of Shell 2 ($a/h = 500$, $a/b = 1$, $b/R = 0.2$): +, constant term; o, first harmonic; □, second harmonic; ◇, third harmonic.

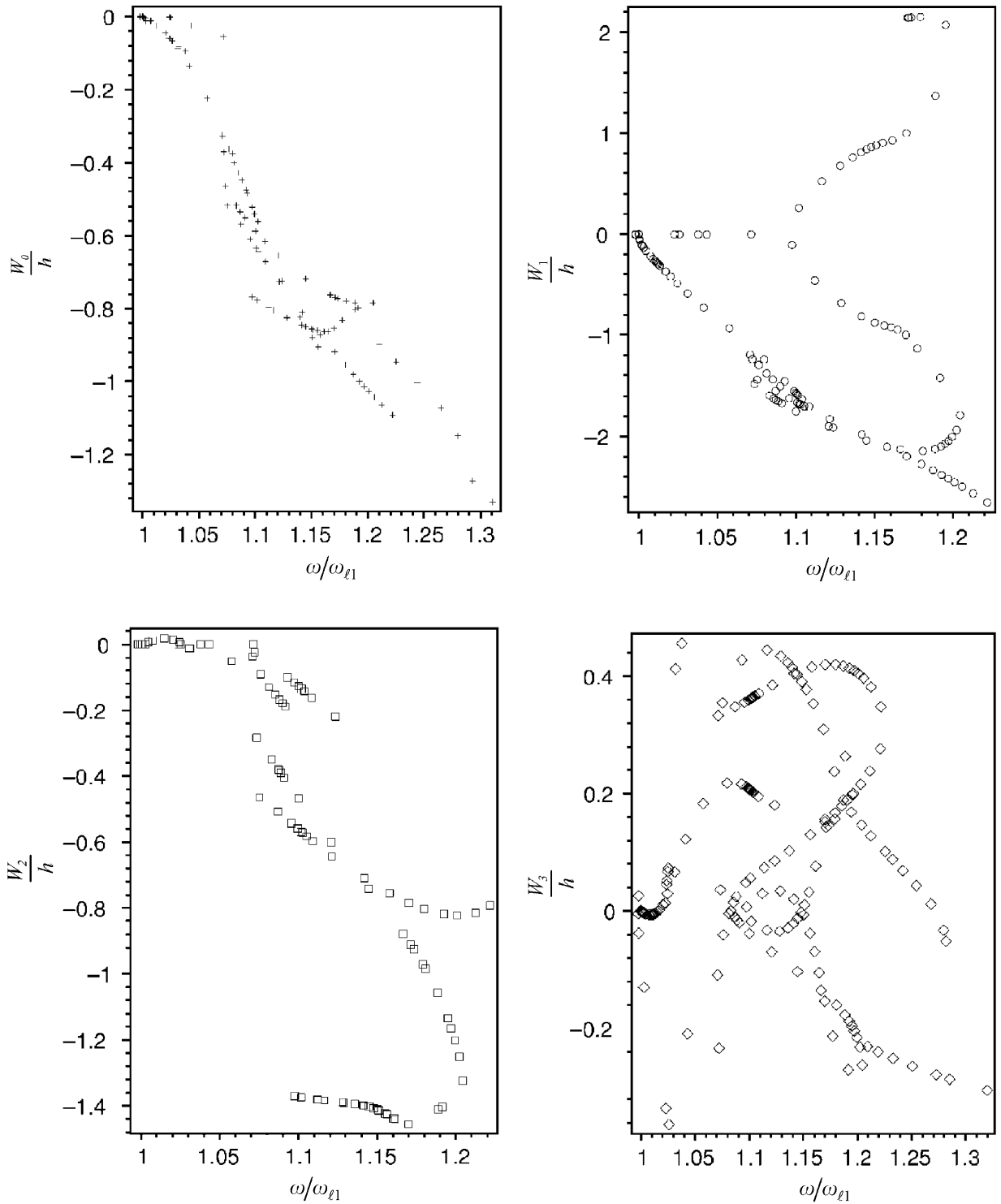


Fig. 8. Backbone curve of Shell 3 ($a/h = 200$, $a/b = 1$, $b/R = 0.4$): +, constant term; ○, first harmonic; □, second harmonic; ◇, third harmonic.

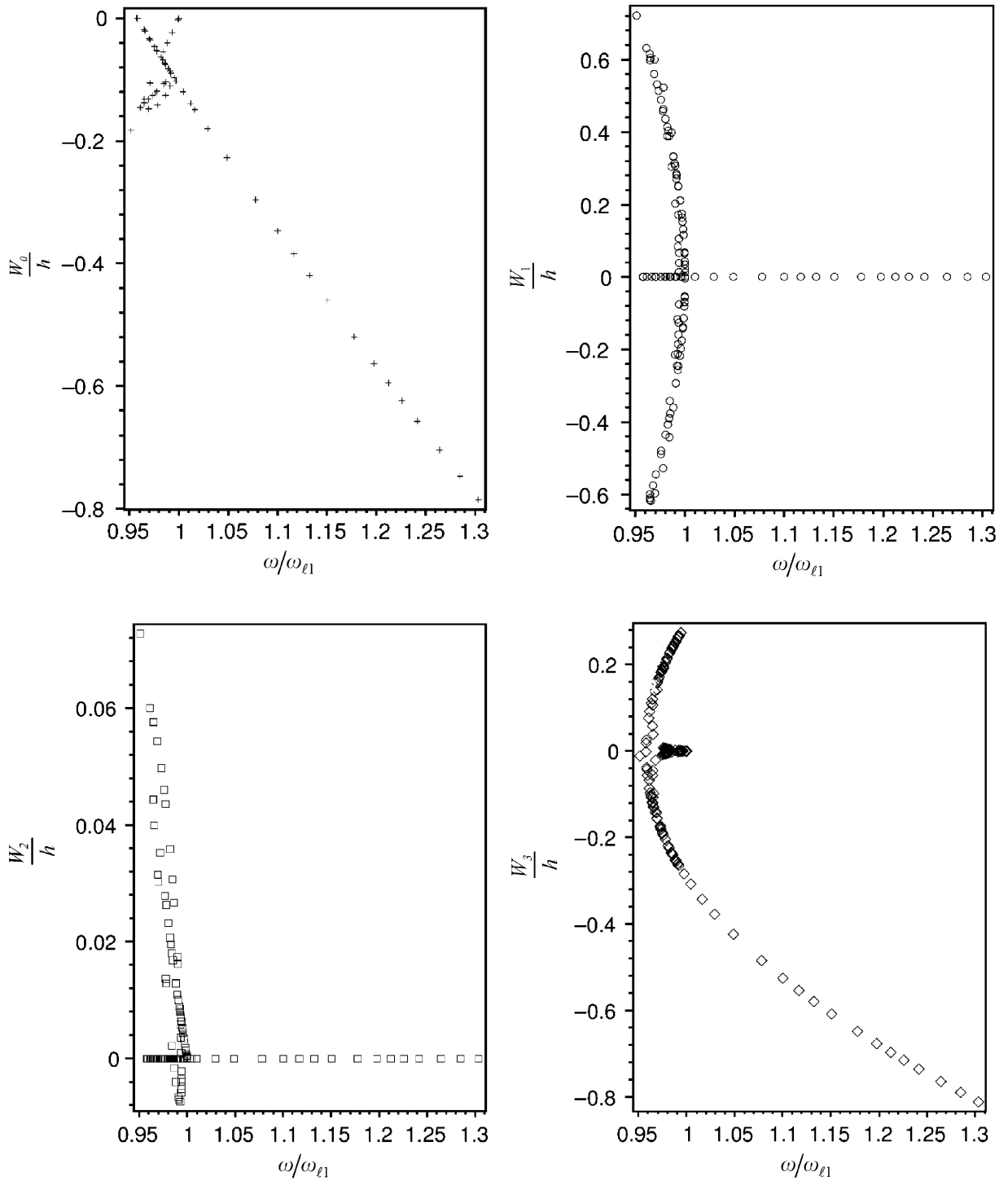


Fig. 9. Backbone curve of Shell 4 ($a/h = 200$, $a/b = 1$, $b/R = 0.2$): +, constant term; o, first harmonic; □, second harmonic; ◇, third harmonic.

For each particular solution, summing the contributions of the harmonics a shape that changes along the vibration period is obtained. An example where the variation of the shape of Shell 1 with time is particularly noticeable is the one shown in Fig. 6. In this figure, the dimensional fundamental frequency is $\omega/\omega_{l1} = 0.989$ and the amplitude of the first harmonic at the central point is $-1.33h$. The shapes of the shell are represented at six instants between $t = 0$ and $T/2$ s, where T represents the period of vibration, after $T/2$ the shapes would repeat in reverse order until arriving at the initial one at $t = T$. As written before, the initial curvature given by Eq. (1) is not represented. The variation of the shape for a given periodic motion is particularly visible in the case of internal resonance, but it is again stressed that the model employed allows to approximately compute non-linear mode shapes—without internal resonance—that change along the vibration period.

Fig. 7 shows the backbone curve of Shell 2, which has a greater initial curvature radius than Shell 1, i.e., Shell 2 is shallower. A wealth of solutions was found, both hardening and softening behaviours are apparent, but hardening dominates. At $(x, y) = (0, 0)$ some solutions only involve the constant term and the second harmonic, others only involve the constant term and the third harmonic, and others involve all harmonics and the constant term. Although the iterations were started at the first linear mode, harmonic motion, higher order modes and strongly non-harmonic oscillations soon appear. Actually, in several solutions the magnitudes of the second and third harmonics are higher than the amplitude of the first harmonic. The differences in the backbone curve of this shell and the deeper Shell 1 are striking and, due to the modal interactions, cannot be simply analysed considering softening versus hardening spring effects.

Fig. 8 shows the backbone curves of Shell 3, a shell which is similar to Shell 1 but thicker. The initial behaviour is hardening, but, as happened with the two previous shells, turning points and several solutions were found in a short frequency span. At $(x, y) = (0, 0)$ most solutions involve all harmonics and the constant term, but different harmonics dominate in different solutions. Similarly to Shell 2, some solutions appeared where the first and second harmonic are identically zero, whilst the constant term and the third harmonic are finite.

The last backbone curve here presented (Fig. 9) is the one of Shell 4, a shell which has the thickness of Shell 3, but larger curvature radius. As with the other three shells, many solutions were found in a short frequency span. Starting from the linear solution, the first harmonic dominates and there is a softening spring effect. Later, hardening spring occurs. The constant term is present in all solutions, in some solutions the first and second harmonics are zero.

4. Final comments

The free periodic non-linear vibrations of cylindrical, open shallow shells were studied with a model that employs a truncated Fourier series to express the time dependence of the solution and is implemented reduction where using linear modes. In spite of these approximations, the model is multi-degree-of-freedom and allows to describe: (1) mode shape variations with maximum vibration amplitude, (2) mode shape variation during a given periodic motion and (3) motions where internal resonance occurs.

Solutions were found that are dominated by one harmonic; however, several harmonics are generally present. The initial curvature and the thickness of the shell determine if the first linear mode is followed by hardening or softening. Internal resonances are apparently very common in undamped shells and the appearance of different modes in the oscillations may swiftly change softening to hardening or vice versa.

Acknowledgement

The author is grateful to Prof. Marco Amabili who provided numerical data to partially validate the model here presented.

Appendix. Linear mode shapes of shell 1

See Fig. A1.

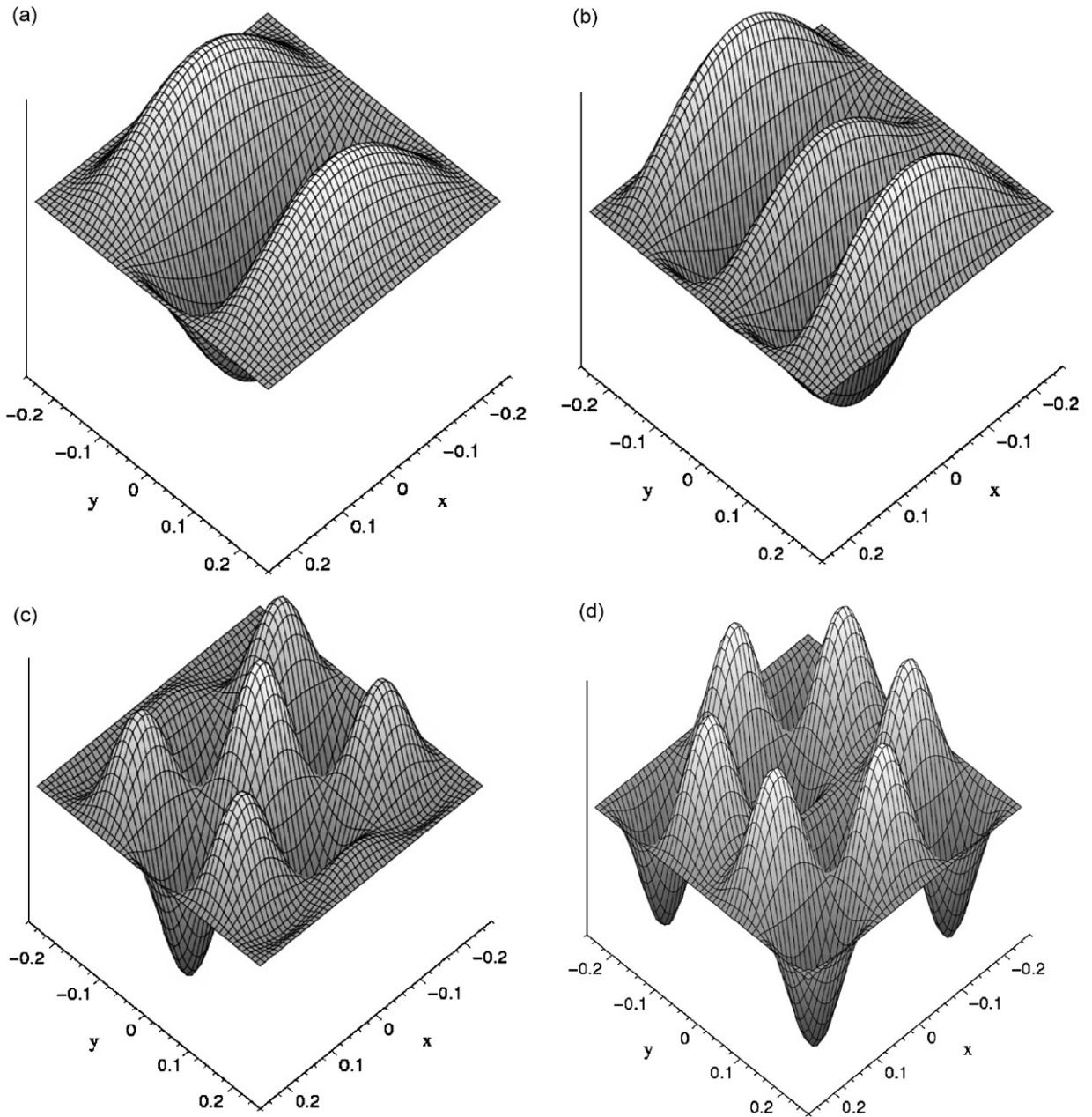


Fig. A1. Linear bi-symmetric modes ordered according to growing linear natural frequencies: (a) mode 1, (b) mode 2, (c) mode 3, (d) mode 4, (e) mode 5, (f) mode 6, (g) mode 7, (h) mode 8, (i) mode 9, (j) mode 10.

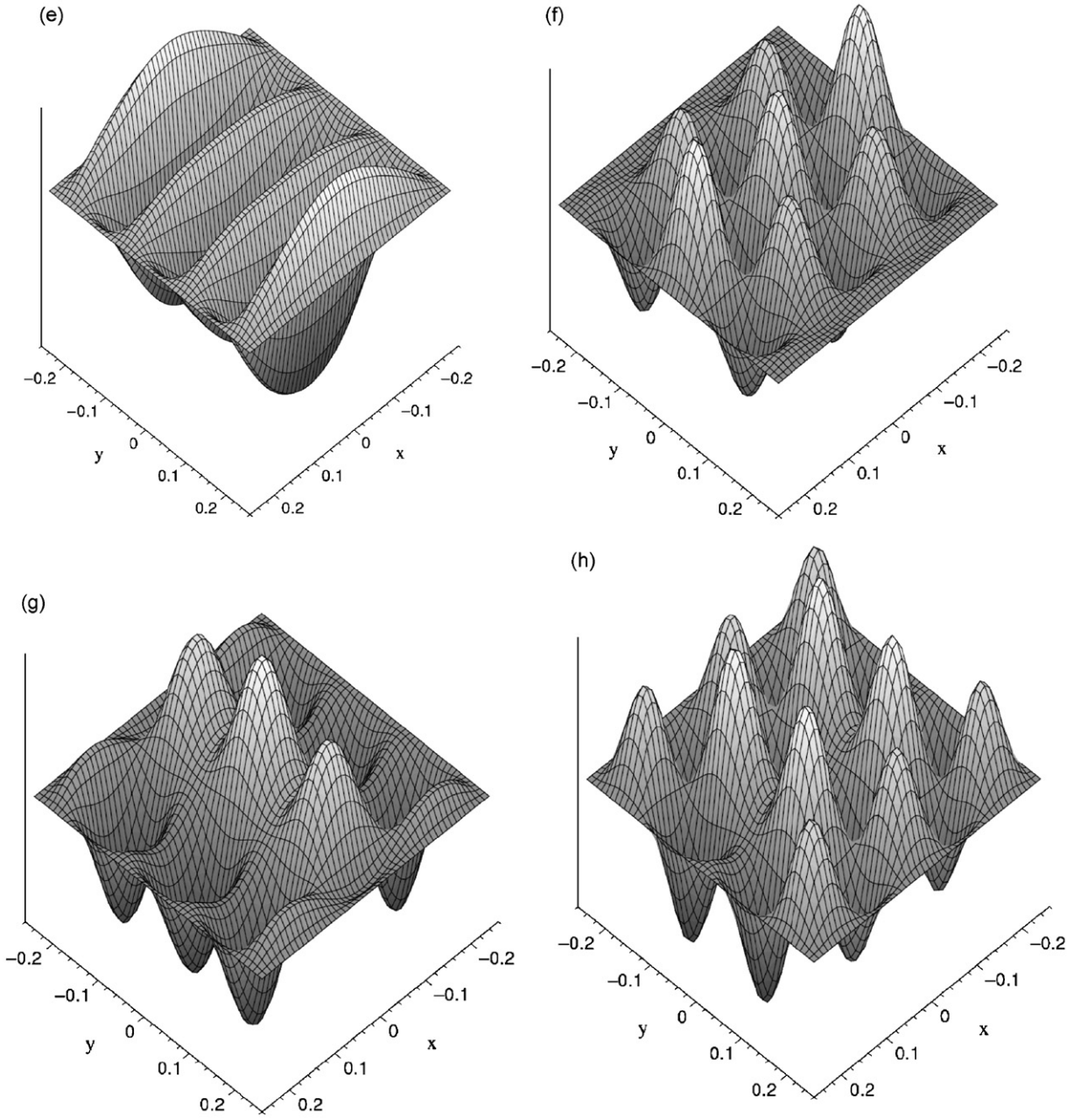


Fig. A1. (Continued)

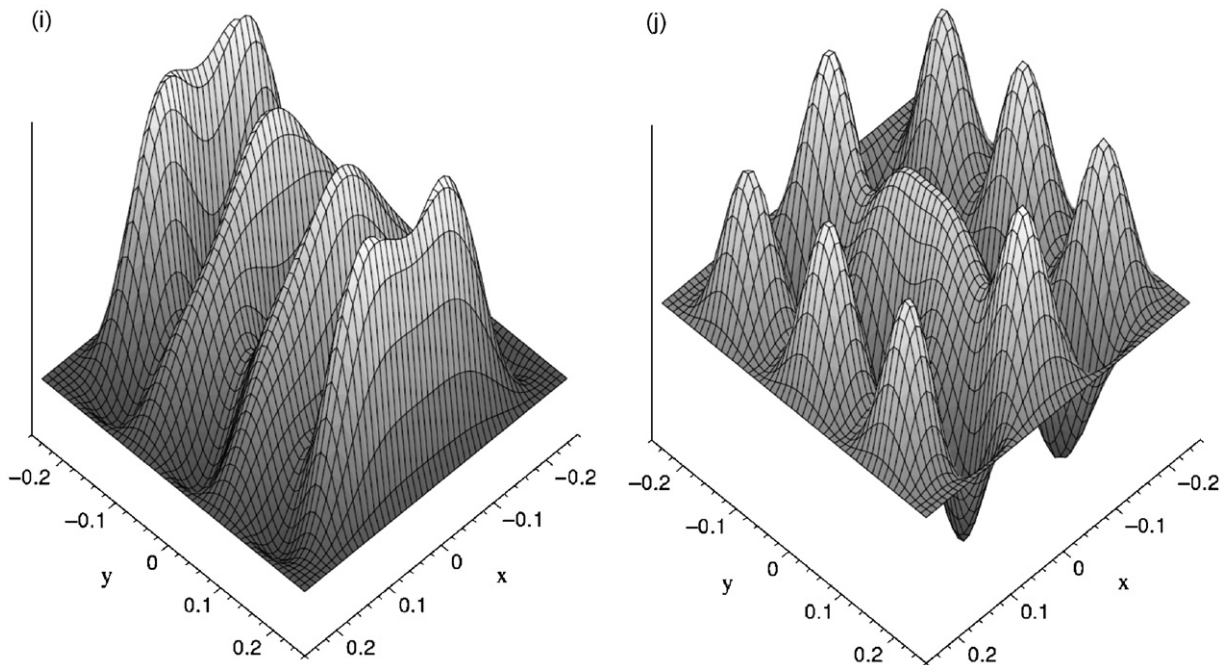


Fig. A1. (Continued)

References

- [1] A.W. Leissa, A.S. Kadi, Curvature effects on shallow shell vibrations, *Journal of Sound and Vibration* 16 (1971) 173–187.
- [2] S.L. Lau, Y.K. Cheung, Amplitude incremental variational principle for non-linear vibration of elastic systems, *Transactions ASME, Journal of Applied Mechanics* 48 (1981) 959–964.
- [3] Y. Kobayashi, A.W. Leissa, Large amplitude free vibration of thick shallow shells supported by shear diaphragms, *International Journal of Non-linear Mechanics* 30 (1995) 57–66.
- [4] S.C. Sinharay, B. Banerjee, Large amplitude free vibration of shallow spherical shell and cylindrical shell—a new approach, *International Journal of Non-linear Mechanics* 20 (1985) 69–78.
- [5] Z.M. Ye, The non-linear vibration and dynamic instability of thin shallow shells, *Journal of Sound and Vibration* 202 (1997) 303–311.
- [6] P. Ribeiro, A hierarchical finite element for geometrically non-linear vibration of doubly curved, moderately thick isotropic shallow shells, *International Journal for Numerical Methods in Engineering* 56 (2003) 715–738.
- [7] A. Przekop, M.S. Azzouz, X. Guo, C. Mei, L. Azrar, Finite element multiple-mode approach to non-linear free vibrations of shallow shells, *AIAA Journal* 42 (2004) 2373–2381.
- [8] M. Amabili, Non-linear vibrations of circular cylindrical panels, *Journal of Sound and Vibration* 281 (2005) 509–535.
- [9] M. Amabili, Theory and experiments for large-amplitude vibrations of circular cylindrical panels with geometric imperfections, *Journal of Sound and Vibration* 298 (2006) 43–72.
- [10] K.M. Liew, K.C. Hung, M.K. Lim, Vibration of shallow shells: a review with bibliography, *Applied Mechanics Reviews* 50 (1997) 431–444.
- [11] M. Amabili, M.P. Paidoussis, Review of studies on geometrically non-linear vibrations and dynamics of circular cylindrical shells and panels, with and without fluid–structure interaction, *Applied Mechanics Reviews* 56 (2003) 349–381.
- [12] W. Han, M. Petyt, Geometrically non-linear vibration analysis of thin, rectangular plates using the hierarchical finite element method-I: the fundamental mode of isotropic plates, *Computers and Structures* 63 (1997) 295–308.
- [13] W. Han, M. Petyt, Geometrically non-linear vibration analysis of thin, rectangular plates using the hierarchical finite element method-II: 1st mode of laminated plates and higher modes of isotropic and laminated plates, *Computers and Structures* 63 (1997) 309–318.
- [14] P. Ribeiro, M. Petyt, Non-linear vibration of plates by the hierarchical finite element and continuation methods, *International Journal of Mechanical Sciences* 41 (1999) 437–459.
- [15] P. Ribeiro, M. Petyt, Non-linear free vibration of isotropic plates with internal resonance, *International Journal of Non-linear Mechanics* 35 (2000) 263–278.
- [16] P. Ribeiro, A hierarchical finite element for geometrically non-linear vibration of thick plates, *Meccanica* 38 (2003) 115–130.

- [17] P. Ribeiro, Modal interactions in shallow shells, in: D.H. van Campen, M.D. Lazaruko, W.P.J.M. van den Oever (Eds.), *Fifth Euromech Nonlinear Dynamics Conference*, Eindhoven University of Technology, 2005.
- [18] E. Ventsel, T. Krauthammer, *Thin Plates and Shells. Theory Analysis and Applications*, Marcel Dekker, New York, 2001.
- [19] M.S. Qatu, *Vibration of Laminated Shells and Plates*, Elsevier, Amsterdam, 2004.
- [20] R. Lewandowski, Computational formulation for periodic vibration of geometrically non-linear structures—part 1: theoretical background, *International Journal of Solids and Structures* 34 (1997) 1925–1947.
- [21] T.D. Burton, M.N. Hamdan, On the calculation of non-linear normal modes in continuous systems, *Journal of Sound and Vibration* 197 (1996) 117–130.
- [22] W. Szemplinska-Stupnicka, *The Behaviour of Non-linear Vibrating Systems*, Kluwer Academic Publishers, Dordrecht, 1990.
- [23] M.M. Bennouna, R.G. White, The effects of large vibration amplitudes on the fundamental mode shape of a clamped–clamped uniform beam, *Journal of Sound and Vibration* 96 (1984) 309–331.
- [24] R. Benamar, M.M.K. Bennouna, R.G. White, The effects of large vibration amplitudes on the mode shapes and natural frequencies of thin elastic structures. Part I: simply supported and clamped-clamped beams, *Journal of Sound and Vibration* 149 (1991) 179–195.
- [25] W. Szemplinska-Stupnicka, “Non-linear normal modes” and the generalized Ritz method in the problems of vibration of non-linear elastic continuous systems, *International Journal of Non-Linear Mechanics* 18 (1983) 149–165.
- [26] S.W. Shaw, C. Pierre, Normal modes of vibration for non-linear continuous systems, *Journal of Sound and Vibration* 169 (1994) 319–347.
- [27] N.S. Bardell, J.M. Dunsdon, R.S. Langley, On the free vibration of completely free, open, cylindrically curved, isotropic shell panels, *Journal of Sound and Vibration* 20 (1997) 647–669.
- [28] A.W. Leissa, Y. Narita, Vibrations of completely free shallow shells of rectangular planform, *Journal of Sound and Vibration* 96 (1984) 207–218.
- [29] R. Seydel, *From Equilibrium to Chaos. Practical Bifurcation and Stability Analysis*, Elsevier Science, New York, 1988.